0026-895X/10/7704-547–558$20.00
MOLECULAR PHARMACOLOGY
Copyright © 2010 The American Society for Pharmacology and Experimental Therapeutics
Mol Pharmacol 77:547–558, 2010

Vol. 77, No. 4
60111/3569909
Printed in U.S.A.

Identification of Determinants of Glucose-Dependent Insulinotropic Polypeptide Receptor That Interact with N-Terminal Biologically Active Region of the Natural Ligand

Tahir Yaqub, Irina G. Tikhonova, Jens Lättig, Remi Magnan, Marie Laval, Chantal Escrieut, Cyril Boulègue, Chandralal Hewage, and Daniel Fourmy

Institut National de la Santé et de la Recherche Médicale, Unit U858, and Université Paul Sabatier (Toulouse III), Toulouse, France (T.Y., I.G.T., J.L., R.M., M.L., C.E., D.F.); Max-Planck-Institut für Biochemie, Martinsried, Germany (C.B.); and Conway Institute, University College Dublin, Dublin, Ireland (C.H.)

Received August 6, 2009; accepted January 8, 2010

ABSTRACT

Glucose-dependent insulinotropic polypeptide receptor (GIPR), a member of family B of the G-protein coupled receptors, is a potential therapeutic target for which discovery of nonpeptide ligands is highly desirable. Structure-activity relationship studies indicated that the N-terminal part of glucose-dependent insulinotropic polypeptide (GIP) is crucial for biological activity. Here, we aimed at identification of residues in the GIPR involved in functional interaction with N-terminal moiety of GIP. A homology model of the transmembrane core of GIPR was constructed, whereas a three-dimensional model of the complex formed between GIP and the N-terminal extracellular domain of GIPR was taken from the crystal structure. The latter complex was docked to the transmembrane domains of GIPR, allowing in silico identification of putative residues of the agonist binding/activation site. All mutants were expressed at the surface of human embryonic kidney 293 cells as indicated by flow cytometry and confocal microscopy analysis of fluorescent GIP binding. Mutation of residues Arg183, Arg190, Arg300, and Phe357 caused shifts of 76-, 71-, 42-, and 16-fold in the potency to induce cAMP formation, respectively. Further characterization of these mutants, including tests with alanine-substituted GIP analogs, were in agreement with interaction of Glu3 in GIP with Arg183 in GIPR. Furthermore, they strongly supported a binding mode of GIP to GIPR in which the N-terminal moiety of GIP was sited within transmembrane helices (TMH) 2, 3, 5, and 6 with biologically crucial Tyr1 interacting with Gln224 (TMH3), Arg300 (TMH5), and Phe357 (TMH6). These data represent an important step toward understanding activation of GIPR by GIP, which should facilitate the rational design of therapeutic agents.

Glucose-dependent insulinotropic polypeptide (GIP; also known as gastric inhibitory polypeptide) is a 42-residue hormone released by the enteroendocrine K cells lining the proximal duodenum (Jörnvall et al., 1981; Moody et al., 1984). GIP stimulates insulin secretion from pancreatic β-cells after ingestion of nutrients. The peptide has a very short half-life in the blood because it is vulnerable to degradation by the ubiquitous enzyme dipeptidyl peptidase IV (Mentlein et al., 1993). GIP, along with its sister incretin hormone glucagon-like peptide 1, has been shown to account for 50 to 70% of postprandial insulin secretion. The incretin effect is strictly glucose-dependent and is essential for the maintenance of glucose homeostasis. GIP further enhances its glucose-lowering effects by the inhibition of hepatic glucose production and the stimulation of proinsulin gene transcription and translation. Because of its hypoglycemic and hypolipidemic effects (Brown, 1974; Baggio and Drucker, 2007), GIP and its receptor (GIPR) are of high pharmacological interest, especially in identification and design of new molecules for the treatment of diabetes mellitus and obesity (Kieffer, 2003). The expression of GIPR in different organs and systems such as stomach, small intestine, adrenal cortex, pituitary, heart, testis, endothelial cells, bone, trachea, spleen, thymus, lung,

This research was supported in part by Association pour la Recherche sur le Cancer [Grant 4870]; and by the Fondation pour la Recherche Médicale (to J.L.).

I.T. and J.L. contributed equally to this work.

Article, publication date, and citation information can be found at http://molpharm.aspetjournals.org.
doi:10.1124/mol.109.060111.

ABBREVIATIONS: GIP, glucose-dependent insulinotropic polypeptide (gastric inhibitory polypeptide); GIPR, glucose-dependent insulinotropic polypeptide receptor; GPCR, G protein-coupled receptor; GL, glucagon; SCT, secretin; VIP, vasoactive intestinal peptide; PTH, parathyroid hormone; ECD, extracellular domain (ectodomain); ECL2, extracellular loop 2; TMH, transmembrane helix; HEK, human embryonic kidney; PCR, polymerase chain reaction; DMEM, Dulbecco's modified Eagle's medium; D-PBS, Dulbecco's phosphate buffered saline; HPLC, high-performance liquid chromatography.

kidney, thyroid, and several regions of the central nervous system increases the pharmacological importance of this receptor (Baggio and Drucker, 2007).

GIPR belongs to subfamily B1 of the G protein-coupled receptor (GPCR) superfamily, which also includes receptors for other hormones [glucagon (GL), glucagon-like peptide 1, glucagon-like peptide 2, secretin (SCT), growth-hormone releasing hormone, vasoactive intestinal peptide (VIP), pituitary adenylate cyclase-activating peptide, corticotropin-releasing factor, parathyroid hormone (PTH), and calcitonin] (Gremlich et al., 1995; Volz et al., 1995). All receptors belonging to this family are composed of a large extracellular N terminus that contains six highly conserved cysteine residues forming three disulfide bridges, a serpentine domain with seven transmembrane helices, and a short intracellular C terminus.

Receptor activation and subsequent intracellular signaling via $G\alpha_s$ protein closely follows the binding of GIP to GIPR (Volz et al., 1995; Baggio and Drucker, 2007). The recent structural characterization of the interaction between GIP and the extracellular domain (ECD; ectodomain) of its receptor demonstrates that GIPR interacts with the C-terminal two thirds of GIP(1–30) peptide (Hinke et al., 2004; Parthier et al., 2007). GIP(1–30) activates GIPR, as demonstrated by intracellular production of cAMP, with potency equal to that of the wild-type peptide GIP(1–42) (Hinke et al., 2001, 2003; Gault et al., 2007). In contrast, fragment GIP(7–30) showed a near maximal affinity with the receptor but had no detectable activity at micromolar concentration. However, fragment GIP(1–14) displayed a very low affinity but fully activated the GIPR at micromolar concentrations (Hinke et al., 2001, 2003; Gault et al., 2007). All together, these data suggest that activation of GIPR by its natural ligand GIP involves high-affinity binding of GIP(7–30) to the N-terminal ECD of GIPR and activating interaction of N-terminal region GIP(1–7) with the GIPR. However, there has been virtually no progress on the delineation of a ligand binding site for the N-terminal region of GIP (i.e., fragment 1–7) to its receptor. As a result, the precise mechanism whereby GIP activates its receptor remains unknown. Understanding ligand binding and receptor activation in GIPR has vital importance in the design of specific high-affinity ligands with a desired pharmacological activity. With this in mind, and based on our experience with cholecystokinin and gastrin receptors (Dufresne et al., 2006), we have initiated this study aimed at the delineation of the binding site of human GIP receptor. Furthermore, given the fact that in family B of the G-protein coupled receptors, little is known about the region of the binding site formed by transmembrane helices, we focused our attention toward this domain of the GIP receptor. Using a strategy combining molecular modeling and site-directed mutagenesis, we identified residues located in transmembrane helices 2, 3, 5, and 6, which are important for GIP recognition by its receptor.

Materials and Methods

Molecular Modeling of GIP Receptor. The sequences of GIP receptors of different species were aligned against other members of subfamily B1 GPCRs to identify conserved hydrophobic regions estimated to be transmembrane helices. The initial model obtained from the multiple sequence alignment was further aligned against the sequence of bovine rhodopsin and A2a adenosine receptors, because the latter was chosen to be the structure template for the serpentine domain (Jaakola et al., 2008). All alignment investigations were done using ClustalX (Chenna et al., 2003). The final sequence alignment is in general agreement with the positioning of transmembrane helices provided by GPCRDB (Horn et al., 2003) (Fig. 1).

The transmembrane helices of GIPR were constructed using side-chain substitutions on the A2a adenosine receptor template (Protein

```
TMH1   GIP-R              VMYTVGYSLSLATLLLALLILSLF
       Adenosine A2a-R    SVYITVELAIAVLAILGNVLVCWA
       Rhodopsin          SMLAAYMFLLIMLGFPINFLTLYV
                                          ^
TMH2   GIP-R              TRNYIHINLFTSFMLRAAAILSRDRLLPRP
       Adenosine A2a-R    VTNYFVVSLAAADIAVGVLAIPFAITISTG
       Rhodopsin          PLNYILLNLAVADLFMVFGGFTTTLYTSLH
                                    ^
TMH3   GIP-R              LAACRTAQIVTQYCVGANYTWLLVEGVYLHSLL
       Adenosine A2a-R    CHGCLFIACFVLVLTQSSIFSLLAIAIDRYIAI
       Rhodopsin          PTGCNLEGFFATLGGEIALWSLVVLAIERYVVV
                                                ^
TMH4   GIP-R              GHFRYYLLLGWGAPALFVIPWVI
       Adenosine A2a-R    TRAKGIIAICWVLSFAIGLTPML
       Rhodopsin          NHAIMGVAFTWVMALACAAPPLV
                                  ^
TMH5   GIP-R              EVKAIWWIIRTPILMTILINFLIFIR
       Adenosine A2a-R    MNYMVYFNFFACVLVPLLLMLGVYLR
       Rhodopsin          NESFVIYMFVVHFIIPLIVIFFCYGQ
                                       ^
TMH6   GIP-R              LARSTLTLVPLLGVHEVVFAPVTEEQ
       Adenosine A2a-R    EVHAAKSLAIIVGLFALCWLPLHIIN
       Rhodopsin          EKEVTRMVIIMVIAFLICWLPYAGVA
                                             ^
TMH7   GIP-R              AKLGFEIFLSSFQGFLVSVLY
       Adenosine A2a-R    WLMYLAIVLSHTNSVVNPFIY
       Rhodopsin          IFMTIPAFFAKTSAVYNPVIY
                                    ^
```

Legend
X = Similar
X = Identical
^ = .50

Fig. 1. Sequence alignment of transmembrane helices for GIP receptor, adenosine A2a receptor, and bovine rhodopsin. The GPCR residue indexing of Ballesteros and Weinstein (1995) is shown.

Data Bank ID 3eml) (Jaakola et al., 2008). External and internal loops were added according to best fit and best homology using a protein template library in Insight II (Accelrys, San Diego, CA). Special attention was paid to the structure generation of extracellular loop 2 (ECL2). Using a disulfide bridge constraint between Cys216 in transmembrane helix (TMH) 3 and Cys286 in ECL2, a structure was selected in which ECL2 is located outside the transmembrane helix bundle, leaving space to accommodate the GIP ligand. Similar to the A2a adenosine receptor template, ECL2 in our model also participates in interactions with ECL1. After refinement of side chain interactions, the model was optimized by steepest descent energy minimization within MOE (Chemical Computing Group, Inc., Montreal, QC, Canada).

For identification of receptor and ligand residues as potential interaction partners, sequences of subfamily B1 receptors of different species as well as sequences of corresponding ligands were aligned separately. Taking into account PTH, corticotropin-releasing factor, calcitonin, and their receptors, remaining ligands and receptors of subfamily B1 were focused in this identification step, because of their closer sequence similarity (especially on ligand side). AnCoRe software package was used for identification of conserved residues as well as correlated mutations (Betancourt and Thirumalai, 1999; Murphy et al., 2000).

In manual docking investigations, the complex structure of GIP bound to the N-terminal ECD of GIPR (Protein Data Bank ID 2qkh) (Parthier et al., 2007) has been used. Taking into account published experimental data on SCT and GL as well as potential interaction sites between peptides and receptors identified in multiple sequence alignment investigations, the complex of GIP-ECD was docked to GIPR. Resulting models, each containing GIP, GIPR ectodomain, and GIPR transmembrane core, were optimized in side-chain interaction and energy. Molecular dynamics simulations using Amber99 force field were applied in MOE for 1 ns to check general reasonability of the formed complex structures.

Site-Directed Mutagenesis of GIPR and Transient Expression in HEK 293 Cells. The plasmid containing the cDNA encoding human GIPR was a kind gift of Professor Bernard Thorens (Lausanne, Switzerland). The sequence encoding the short variant of the GIPR was PCR-amplified using a sense primer containing cloning site HindIII as well as a sequence encoding the hemagglutinin epitope tag YPYDVPDYA, and an antisense primer containing cloning site XhoI. PCR product was subcloned in pcDNA3 and sequenced. All mutants were constructed by oligonucleotide-directed PCR-based mutagenesis using human GIPR cDNAs cloned in the pcDNA3 vector as a template. The presence of desired mutation and the absence of undesired mutation were confirmed by automated sequencing of the complete GIPR coding sequence. HEK 293 cells (2.5×10^6) were plated onto 10-cm culture dishes and grown in Dulbecco's modified Eagle's medium (DMEM) containing 10% fetal calf serum in a 5% CO_2 atmosphere at 37°C. After overnight incubation, cells were transfected with 12 μg/culture dish of pcDNA3 vector containing the cDNA for the wild-type or mutated GIP receptor, using FUGENE 6 reagent in DMEM. The medium was aspirated 24 h later and was replaced with fresh medium with serum.

cAMP Production by HEK 293 Cells Expressing GIP Receptors. Approximately 24 h after the addition of fresh DMEM and after overnight incubation, the transfected cells were rinsed with Dulbecco's phosphate buffered saline (D-PBS). Cells were detached by scraping in the presence of 10 ml of D-PBS and incubated at 37°C for 15 min with 0.25 mM 3-isobutyl-1-methylxanthine. Approximately 5×10^4 cells in a volume of 180 μl were stimulated by 20 μl of peptide [GIP(1–30) or Ala-substituted GIP(1–42)] in an increasing concentration from 10 pM to 10 μM, in duplicate tubes. To measure basal cAMP production, 180 μl of cells were added to 20 μl of D-PBS. All samples were incubated for 15 min at 37°C. Reactions were stopped on ice and by addition of 800 μl of 95:5 methanol/formic acid. Tubes were capped, vortexed, and left at −20°C overnight. The next morning all the samples and radioimmunoassay cAMP kit (Immunotech, Marseille, France) were allowed to come to room temperature, and the reagents were reconstituted. Samples or calibrators were added to anti-cAMP antibody-coated tubes in the presence of 500 μl of ^{125}I-labeled cAMP tracer and incubated at 4°C for 18 h. Bound radioactivity was directly measured in a gamma counter (Packard Auto-Gamma, PerkinElmer Life and Analytical Sciences, Waltham, MA). Data were analyzed and graphs drawn up by using the nonlinear curve-fitting software Prism (GraphPad, San Diego, CA).

Synthesis and Purification of GIP(1–30) Amide. The machine-assisted stepwise solid phase peptide synthesis was carried out on a Pioneer Peptide Synthesis System (Applied Biosystems, Foster City, CA) using the standard procedures of 9-fluorenylmethoxycarbonyl/*tert*-butyl chemistry on a TentaGel S RAM resin from Rapp Polymere GmbH, Tübingen, Germany), and the crude peptide was obtained after a 2-h treatment with trifluoroacetic acid/triisopropylsilane/H_2O (95:2.5:2.5) followed by precipitation in an ice-cold solution of methylbutylether/hexane (2:1). The compound was isolated by preparative HPLC using a C8 column (5 mm, 250 × 21 mm) and mass spectrometry [electrospray ionization-mass spectrometry: m/z = 1767.0 $[M + 2H]^{2+}$, 1178.2 $[M + 3H]^{3+}$, 884.0 $[M + 4H]^{4+}$; 3532.02 calculated for $C_{162}H_{240}N_{40}O_{47}S$]. Analytical HPLC confirmed peptide purity.

Preparation of GIP-Alexa Fluor 647. Coupling of GIP(1–30) to Alexa Fluor 647 was carried out by mixing, at 20°C, 20 nmol of GIP in solution in 0.1 M sodium borate, pH 8.5, with 100 nmol of Alexa Fluor carboxylic acid succinimidyl ester (Invitrogen, Carlsbad, CA) in solution in dimethyl formamide. After 6 h of reaction, the solution was submitted to HPLC separation on a Nucleosil C18 column (Bischoff, Leonberg, Germany) using a linear gradient of acetonitrile from 25 to 50% of acetonitrile in H_2O/0.05% trifluoroacetic acid (Fig. 4).

Determination of Expression Levels of GIP Receptors. HEK 293 cells (2×10^5) were cultured and transfected as described above. The cells were rinsed once with complete medium, detached in 1 ml of complete medium, and transferred to special plastic tubes for flow cytometry analysis. The cells were rinsed by centrifugation at 1000× rpm for 3 min at 4°C in the presence of 2 to 3 ml of 0.5% bovine serum albumin-phosphate buffer solution and then resuspended in 100 μl of incubation buffer. After an initial incubation for 10 min at room temperature, GIP-Alexa Fluor 647 was added with a final concentration of 10 μM to the cells and incubated for 1 h at room temperature in the dark. The cells were rinsed twice by centrifugation and resuspended in 0.5 ml of incubation buffer and were analyzed by the flow cytometry (FACSCalibur; BD Biosciences, San Jose, CA). The data were analyzed using Cell Quest Pro software with reference to both positive control (i.e., cells expressing wild-type GIPR) and negative control (i.e., nontransfected cells). For confocal microscopy visualization of GIPR expression, cells were grown on sterile four-well Lab-Tek cover glass chambers (Nunc; Thermo Fisher Scientific, Roskilde, Denmark) coated with polylysine and incubated at 4°C for 2 h with 1 μM GIP-Alexa Fluor 647 in D-PBS before observation using a confocal microscope [LSM 510 (Carl Zeiss GmbH, Jena, Germany); excitation at 633 nm by argon laser and emission >650 nm]. Background-subtracted images were assembled using Adobe Photoshop 7.0 (Adobe Systems, Mountain View, CA).

Results

Identification of Putative Binding Site of GIP Receptor by Molecular Modeling and In Silico GIP Docking. Based on multiple sequence alignments of both receptors and ligands, we constructed models of the GIPR-GIP complex using adenosine A2a receptor as a template for the receptor's transmembrane helix bundle and taking X-ray structural data on the interaction of GIP and GIPR ECD into account (Parthier et al., 2007). Thereby, two binding modes showed reasonable interactions (Fig. 2).

In docking model A (Fig. 2a) GIP interacts with GIPR in a fashion similar to a binding mode proposed for glucagon in glucagon receptor (Runge et al., 2003): the N terminus of GIP is oriented in the direction of TMH1 of GIPR, leaving residues Ala2 and Glu3 between TMH2 and TMH7, whereas the GIP helical structure lies on the receptor, establishing contacts with ECL2 and ECL3. In this first model, Arg183 and Arg190 in TMH2 (Fig. 3) interact with Glu3 of GIP, and Arg300 in TMH5 interacts with Asp15 of GIP. These interactions have been identified as important in this first binding mode and thus selected for mutation.

In docking model B (Fig. 2b) GIP interacts in GIPR in a fashion similar to that described for the binding of secretin to secretin receptor (Dong et al., 2008): the N terminus orients toward ECL3, allowing residues between it and the GIP helical portion to find interactions within a binding groove made up of TMH 2, 3, 5, 6, and 7. Similar to binding model A, binding model B depends on interaction between Arg183 in TMH2 and Glu3 of GIP (Fig. 3). In contrast, Tyr1 and Ala2 of GIP established additional interactions within a typical GPCR ligand binding pocket. Residues Gln220, Thr223, and Gln224 in TMH3, Arg300 in TMH5, and Phe357 in TMH6 have been predicted for experimental investigation to validate binding model B. In addition and independently of the two described putative binding modes, we were interested in identifying residues with importance in receptor activation. Because of their close proximity to Arg183 (TMH2) and the possibility of establishing a hydrogen bond network inside the receptor, residues Asn230 (TMH3), Tyr231 (TMH3), His353 (TMH6), and Gln384 (TMH7) have been proposed for experimental investigation. The appearance of residues Asn230, Tyr231, and His353 in class B GPCRs seems to be related to Arg183 in TMH2. In contrast, Gln384 in TMH7 is one of the most conserved residues within all class B GPCRs, and its corresponding residue in PTH/PTH-related protein receptors has been shown to be critical for ligand binding and receptor activation (Gardella et al., 1996).

We also proposed residue Tyr392 in TMH7 for investigation. This residue is not near any putative residue of the GIPR binding site. However, our sequence alignment investigations indicated that this residue corresponds to tyrosine in NPxxY motif, which has been demonstrated to be involved in activation of members of class A GPCRs (Gether, 2000).

Biological Characterization of GIP-Alexa Fluor 647 and Expression of GIPR Mutants. Synthetic fragment 1–30 of GIP was coupled to Alexa Fluor succinimidyl ester, and the coupling medium was submitted to reversed-phase HPLC. According to mass spectrometry analysis of trypsin-digested fragments and N-terminal amino acid determination (data not shown), compound contained in the major peak eluted at 16.5 min corresponded to GIP coupled to Alexa Fluor through Lys30 (Fig. 4a). GIP-Alexa Fluor 647 thus purified stimulated cAMP formation in HEK 293 cells expressing the GIPR with potency and efficacy similar to that of GIP(1–30) (Fig. 4b). GIP-Alexa Fluor 647 was further used for measurement of GIPR mutant expression at the cell surface, which might be affected by site-directed mutagenesis substitution of residues in the GIPR. In the first series of experiments, batches of cells expressing the different mutants were incubated with GIP-Alexa Fluor 647 at a saturating concentration (1 μM) and analyzed by flow cytometry. Values from fluorescence-activated cell sorting profiles indicated that all mutants were expressed at HEK 293 cell membrane at levels similar to that of the wild-type GIPR (Table 1). In a second series of experiments, cells plated on microscope Lab-Tek cover glass chambers were incubated on ice with GIP-Alexa Fluor 647 (1 μM) and observed by confocal microscopy. Photomicrographs shown in Fig. 5 demonstrated that all mutants were expressed at the HEK 293 cell surface and at levels comparable with that of the wild-type GIPR.

Pharmacological and Site-Directed Mutagenesis Identification of Amino Acids Involved in GIP-Induced cAMP Production. We further aimed to pharmacologically test our proposed models for binding of GIP to GIPR. Main

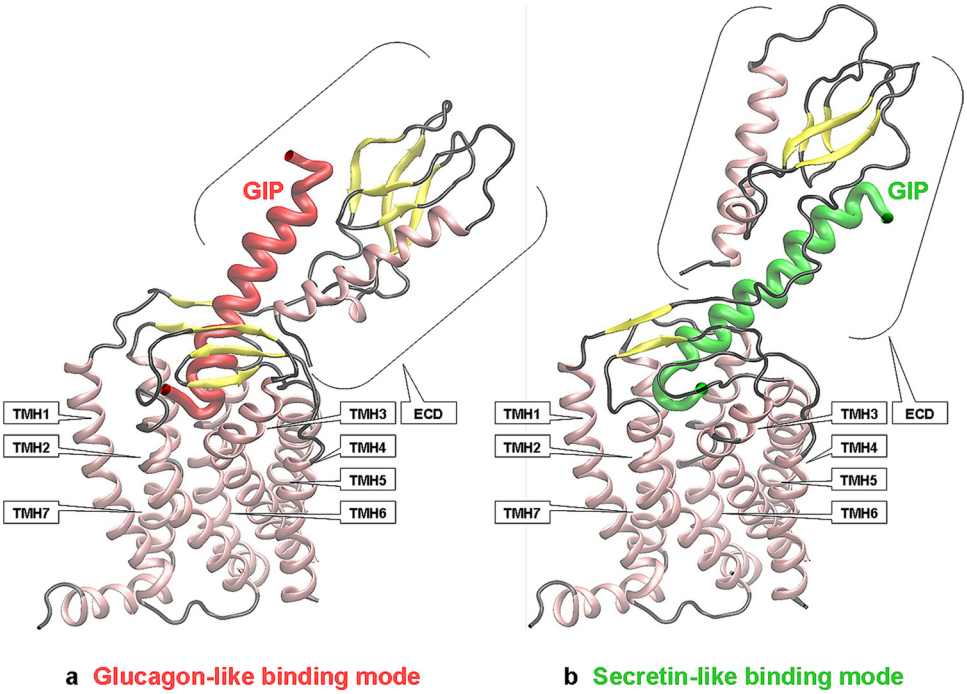

Fig. 2. Schematic representation of theoretical docking modes of GIP to the GIP receptor. Molecular docking investigations resulted in two different potential binding modes of GIP in GIPR. The binding modes resemble the differently described receptor ligand interactions for homologous class B GPCRs GL-R and SCT-R. Although the complex of GIP and GIPR ECD shows different orientations regarding the transmembrane helix bundle, both models showed reasonable contact sites.

residues identified in these different three-dimensional models, namely Arg183, Arg190, Gln220, Thr223, Gln224, Asn230, Tyr231, Arg300, His353, Phe357, Gln384, and Tyr392 were each exchanged for an alanine, Gln384 for an asparagine, and Tyr231 for a phenylalanine. Performing activity assays on HEK 293 cells expressing these mutants allowed identifying positions important in ligand-induced receptor activation by shifts in potency of measured cAMP-production (Fig. 6 and Table 1).

The biggest influence of alanine substitution on GIP po-

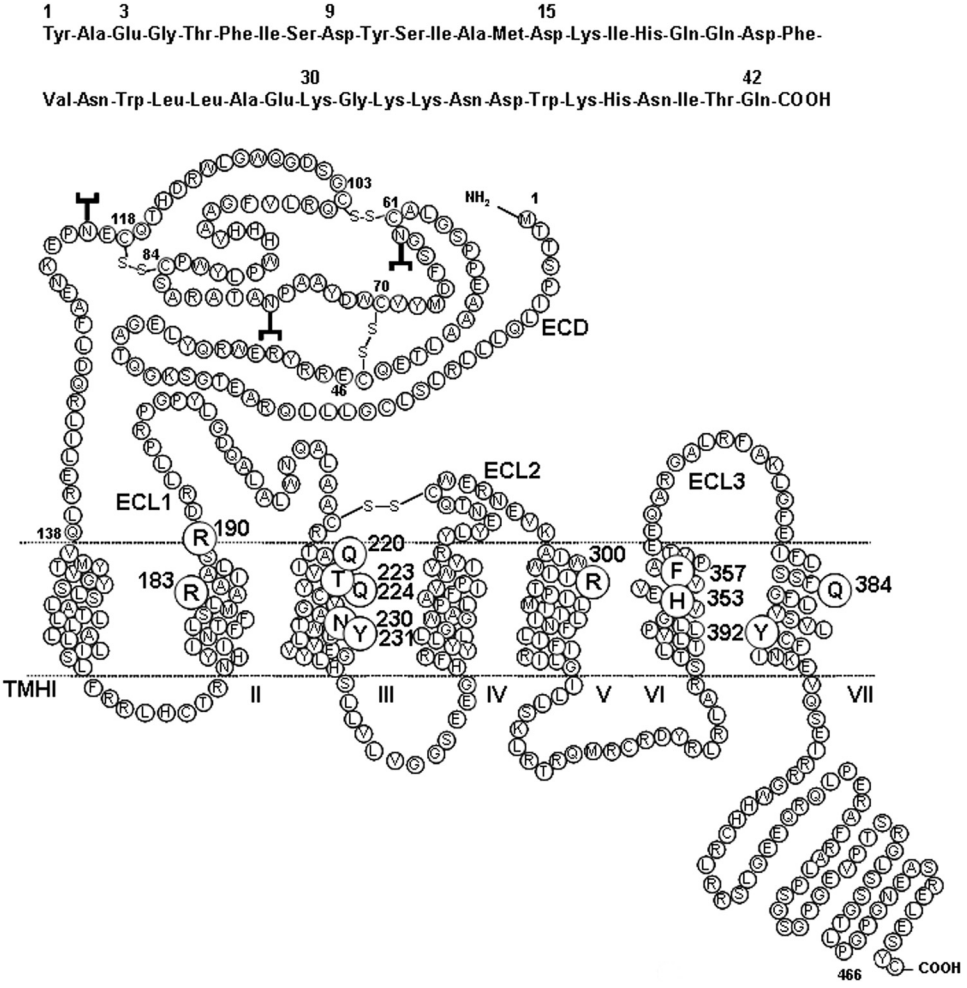

Fig. 3. Primary structure of GIP and serpentine representation of GIP receptor. In the upper part of the figure, amino acid sequence of GIP is given. In the serpentine representation of the human GIPR, residues that have been mutated (circled letters), extracellular domain (ECD), extracellular loops (ECL1, ECL2, ECL3), and transmembrane helices (TMHI-VII) are depicted.

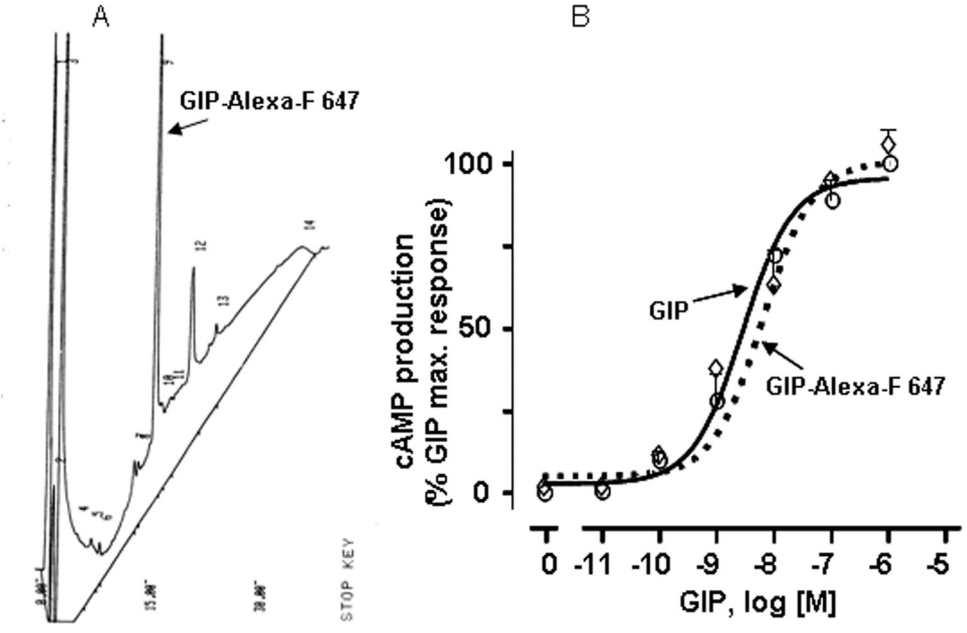

Fig. 4. Preparation and biological activity of GIP-Alexa Fluor 647. A, high-performance liquid chromatography purification of GIP-Alexa Fluor 647. The separation was performed as described under *Materials and Methods*. Absorption peak 9 (280 nm) eluted at 16.0 min corresponded to GIP coupled to Alexa Fluor 647 through Lys30. B, biological activity of GIP-Alexa Fluor 647. GIP- or GIP-Alexa Fluor 647-induced cAMP production was measured in HEK 293 cells expressing the human GIP receptor. Results are expressed as percentage of maximum cAMP production in the presence of GIP. EC_{50} values were 2.9 and 5.7 nM for GIP and for GIP-Alexa Fluor 647, respectively ($n = 2$).

tency was discovered for R183A (F_{mut} 76.4, $p < 0.001$) and R190A (F_{mut} 71.2, $p < 0.001$), both located in TMH2. Important decreases in potency were also found for R300A in TMH5 (F_{mut} 42.0) and F357A in TMH6 (F_{mut} 15.7). Furthermore, significant decreases ($p < 0.001$) were observed for Q220A, T223A, Q224A and N230A, all in TMH3 (Table 1). In contrast, minor influence has been noticed for Tyr231 (TMH3), His353 (TMH6), Gln384 (TMH7), and Tyr392 (TMH7). Efficacy (maximum cAMP production) by which all mutants responded to GIP was near that of the wild-type receptor (Table 1).

Pharmacological Discrimination between the Theoretical Models A and B of GIPR-GIP Complex. To discriminate between the two theoretical docking models for GIPR-GIP complexes, we aimed at identification of interacting charged amino acids in both the GIPR and GIP as we described previously for cholecystokinin receptors (Gigoux et al., 1999; Silvente-Poirot et al., 1999). A pharmacological support for the interactions was first based on the assumption that mutation of putative interacting amino acids in GIP and in GIPR should cause equivalent shifts in potency in cAMP production. To further assess the interaction, we reasoned that simultaneously mutating the interacting amino acids in GIP and GIPR should not further shift the potency in cAMP production relative to single mutations on either GIP or GIPR. On the contrary, simultaneous exchange of residues that do not interact should induce an additional decrease in the potency relative to single mutations on either GIP or GIPR.

In the two models (A and B) of the GIPR-GIP complex, Arg183 in TMH2 (Fig. 3a) interact with Glu3 of GIP. On the other hand, Arg183 and Arg190 are only two helix turns distant from each other, which is comparable with the distance of Glu3 and Asp9 in GIP, suggesting that Arg190 interacts with Asp9. Therefore, we first determined the influence of E3A and D9A substitution in GIP. As illustrated in Fig. 7, potency of GIP to stimulate R183A GIPR was identical to potency of Ala3 GIP to stimulate the wild-type GIPR. In addition, no further significant decrease in potency was seen when Ala3 GIP was used to stimulate R183A GIPR. This strongly supports the idea that Arg183 directly and uniquely interacts with Glu3 of GIP to induce cAMP formation. In contrast, Ala9 GIP at concentrations up to 10 μM did not stimulate cAMP production through R183A-GIPR suggesting no direct interaction between Arg183 and Asp9 of GIP.

As for Arg190, experiments shown in Fig. 8 indicate that E3A substitution in GIP and R190A substitution in GIPR result in equal decrease in potency. However, simultaneous mutations in ligand and receptor produced an additional dramatic shift in potency relative to the single alanine substitutions ($EC_{50} > 10$ versus 0.1 μM), as well as a dramatic decrease in cAMP production level. On the other hand, potency of GIP to stimulate R190A-GIPR was very close to the potency of Ala9 GIP to stimulate wild-type GIPR, but Ala9 GIP did not stimulate R190A-GIPR. All together, these data allow us to conclude that direct interactions taking place between Arg190 in GIPR and Glu3 in GIP or between Arg190 in GIPR and Asp9 of GIP are very unlikely.

One major difference between the two theoretical binding modes A and B concerns Arg300 in the GIPR, which interacts with Asp15 of GIP in model A and with Tyr1 of GIP in model B. Furthermore, another important difference concerns the Tyr-Ala sequence of GIP, which lies on the GIPR surface in model A, whereas it interacts more deeply in the binding pocket with Phe357, Arg300, Gln220, Thr223, and Gln224 in model B. It is also worth specifying that in model A, Glu3 is near Arg300 and Phe357. However, charge interactions between Arg300 and Glu3 of GIP were not recognized, because the Phe357 benzene ring interferes between both charged residues.

We therefore first analyzed experimentally the possible interactions between Arg300 and Glu3 of GIP as well as with other negatively charged residues in GIP, namely Asp9 and

TABLE 1

Effect of mutation of human GIPR on its expression and ability to induce cAMP formation

Receptor expression was measured by flow cytometry using GIP-Alexa F 647 as label of GIPR. Results are expressed as percentage of expression value of the WT-GIPR and are the means ± S.E.M. of three or four individual experiments. F_{mut} (mutation factor) was calculated as EC_{50} (mutated GIPR)/EC_{50} (WT-GIPR), where EC_{50} is the potency of GIP (based on four to nine determinations). E_{max} corresponds to efficacy of GIP to stimulate cAMP production. E_{max} values are expressed as percentage of GIP-stimulated cAMP production with the WT-GIPR.

GIP-R	Location	Receptor Expression	cAMP production		
			EC_{50}	F_{mut}	E_{max}
		%	*nM*		%
WT		100	1.96 ± 0.32		100
Mutant R183A	TMH II	76.1 ± 4.6	149.7 ± 30.8***	76.4	84.2 ± 9.5
Mutant R190A	TMH II	84.9 ± 6.7	139.3 ± 16.8***	71.2	81.7 ± 7.1
Mutant Q220A	TMH III	110.2 ± 1.1	9.2 ± 4.3***	4.7	99.0 ± 7.0
Mutant T223A	TM III	116.9 ± 17.0	6.7 ± 2.6***	3.4	100.3 ± 5.1
Mutant Q224A	TM III	77.2 ± 7.6	11.0 ± 5.0***	5.6	117.0 ± 6.7
Mutant N230A	TM III	91.9 ± 0.7	12.7 ± 1.2***	6.5	98.1 ± 6.8
Mutant Y231A	TM III	102.5 ± 1.7	4.2 ± 0.9*	2.1	114.5 ± 15.2
Mutant Y231F	TM III	96.2 ± 8.1	7.9 ± 4.8**	4.0	101.2 ± 7.8
Mutant R300A	TM V	75.1 ± 6.5	82.3 ± 15.9***	42.0	85.8 ± 3.8
Mutant H353A	TM VI	96.5 ± 8.7	2.5 ± 1.7	1.3	130.9 ± 8.9
Mutant F357A	TM VI	77.0 ± 6.1	30.8 ± 9.3***	15.7	114.1 ± 11.7
Mutant Q384A	TM VII	115.3 ± 3.4	5.2 ± 1.4**	2.6	111.5 ± 23.0
Mutant Q384N	TM VII	109.4 ± 9.7	3.2 ± 1.6	1.6	115.8 ± 15.8
Mutant Y392A	TM VII	89.9 ± 3.9	9.5 ± 4.0***	4.8	106.8 ± 13.2
R1831.Q384A-GIPR	TMII-VII	12.0 ± 0.2	32.5 ± 12.3**	16.6	28.0 ± 10.2

* $P < 0.05$ evaluated by Student's t test compared with wild-type receptor value.
** $P < 0.01$ evaluated by Student's t test compared with wild-type receptor value.
*** $P < 0.001$ evaluated by Student's t test compared with wild-type receptor value.

Asp15. Results from these experiments are shown on Fig. 9. Alanine substitution of Glu3, Asp9, or Asp15 caused 28-, 35-, and 20-fold decreases, respectively, in the potency of GIP to stimulate the wild-type GIP receptor (experiments shown in Figs. 7–9). Substitution R300A in the GIPR decreased by 42-fold the potency with which the receptor responded to GIP (Table 1, Fig. 6). Double mutations in both GIP at position 3, 9, or 15 and in GIPR at position Arg300 caused further dramatic shifts in cAMP production potency relative to single substitution either on the peptide or on the receptor, supporting the concept that none of the three acidic amino acids of GIP (Glu3, Asp9, and Asp15) interacts with Arg300. As a result, docking model A is not supported by experimental data concerning R300A. In contrast, decrease in potency found for R300A and F357A mutants (F_{mut} 42.0 and 15.7, respectively) together with those observed with Q220A, T223A, Q224A, and N230A mutants, all in TMH3 (F_{mut} 4.7, 3.4, 5.6, and 6.5, respectively; Table 1), clearly support the model of a GIP-GIPR complex corresponding to docking model B.

Finally, because in the PTH2 receptor the residue equivalent to Arg183 in GIPR was shown to be functionally linked to the residue equivalent to Gln384 in GIPR (Gardella et al., 1996), we double-mutated GIPR at the two positions: 183 and 384. Double mutation R183A-Q384A decreased the efficacy (75%) and the potency (14-fold) by which the GIPR responded to GIP to stimulate cAMP production (Fig. 10). It is noteworthy that shift of potency caused by the double mutation was smaller than that caused by the single mutation R183A (16.6- versus 76.4-fold; Fig. 10). Expression experiments indicated that the double mutant was significantly less expressed at the cell surface than the wild-type GIP (12% of wild-type GIPR expression; data not shown) suggesting that the apparent decrease in cAMP production was solely caused by the drop in expression of the double-mutant.

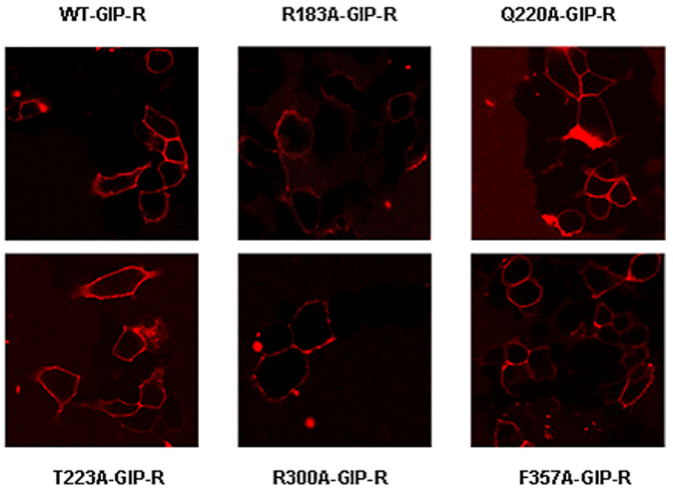

Fig. 5. Expression of GIP receptors in HEK 293 cells. For quantification of expression and visualization of wild-type and mutated GIPR, transfected cells were incubated with 0.1 to 1 μM GIP-Alexa Fluor 647 and analyzed by flow cytometry or observed by confocal microscopy as described under *Materials and Methods*. Representative microscopy pictures are shown for only six GIPR variants, but expression of all GIPR mutants at the cell surface of HEK 293 cells was visualized.

Description of the Binding Pocket in GIP Receptor Involved in Interaction with N-Terminal Moiety of GIP for Identified Binding Model B. In binding model B (Fig. 11), which is strongly supported by pharmacological data, GIP rests with its C terminus bound to the ECD in a binding grove between ECL2 and ECL3. This way, residues of the GIP N-terminal portion (residues 1 to 5) find interactions within the transmembrane helix bundle.

In detail, Tyr1 of GIP establishes a hydrogen bond to Gln224 (TMH3) and π-cation interaction to the guanidino group of Arg300 (TMH5). In addition, Tyr1 rests in a hydrophobic pocket consisting of Ile295 (TMH5), Val360 (TMH6), and Phe357 (TMH6). These interactions are in agreement with the shifts in potency for cAMP production resulting from alanine substitution of these residues in GIPR: Gln224 (5.6-fold), Arg300 (42-fold), and Phe357 (15.7-fold). The methyl

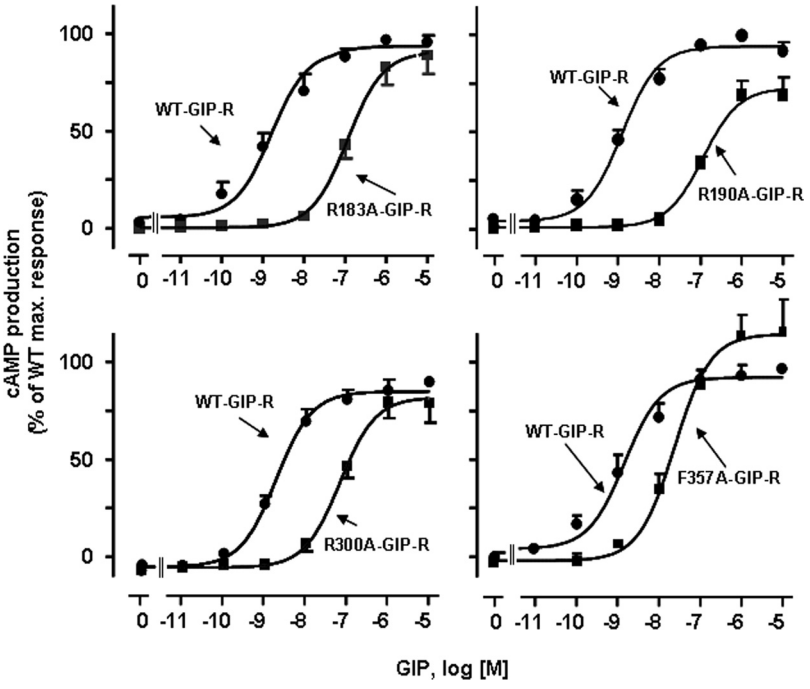

Fig. 6. Importance of residues Arg183, Arg190, Phe357, and Arg300 in the GIP receptor for GIP-induced cAMP production. Wild-type GIP receptor or mutants R183A, R190A, F357A, or R300A were expressed in HEK 293 cells and stimulated for 15 min by GIP for cAMP production measurement. Mutation factors (Fwt) were calculated as EC_{50} (mutated GIPR)/EC_{50} (WT-GIPR). E_{max} values are expressed as percentage of wild-type receptor maximal cAMP production in response to 1 μM GIP. Cell surface expression of the mutants of the GIPR was assessed by flow cytometry using GIP-Alexa Fluor 647 as ligand and was expressed as percentage of the value achieved with wild-type GIPR. Results represent the means ± S.E.M. of at least four independent experiments performed in duplicate on separately transfected HEK 293 cells. Calculated EC_{50} values are reported in Table 1.

side chain of Ala2 in GIP finds a corresponding environment in TMH3 close to Gln220 and Thr223. Glu3 of GIP interacts with Arg183 (TMH2). The interaction is based on charge polarized hydrogen bonds. We also recognized the possibility of hydrogen bonding between Glu3 backbone NH with the side chain carbonyl of Gln220 (TMH3) during MD simulation (interaction not shown). Residue Gly4 of GIP is not involved in direct receptor ligand interactions, but its small size allows a close orientation to TMH1 in the narrow space between TMH2 and TMH7.

We further suggest the necessity of the formation of a turn-like structure in the GIP N terminus while interacting in GIPR: Ala2 backbone carbonyl oxygen is involved in hydrogen bonding to the backbone NH of Thr5 of GIP, which in return caps the N terminus of GIP central helix moiety via its side chain. In addition, the flexible character of Gly4 sup-

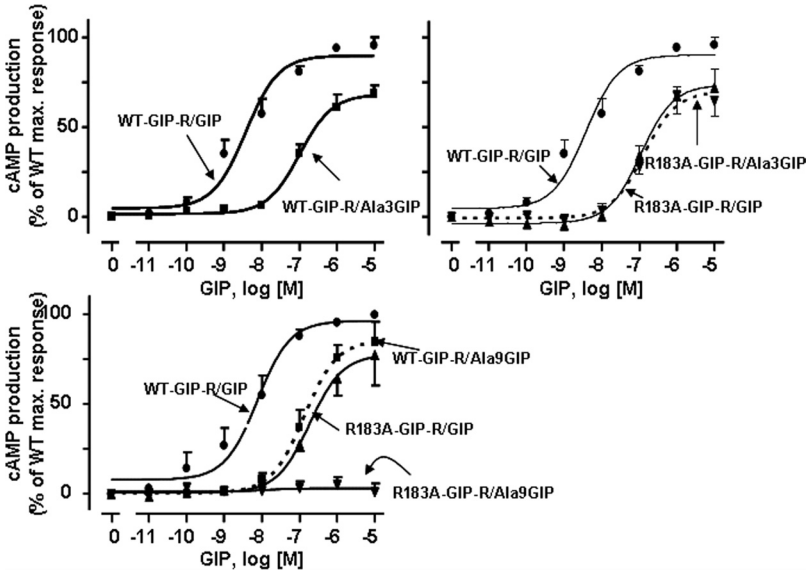

Fig. 7. Pharmacological evidence for a direct interaction between of Arg183 of GIPR and Glu3 of GIP but not Asp9. Wild-type GIP receptor or mutant R183A-GIPR were expressed in HEK 293 cells and stimulated for 15 min either by GIP, Ala3-GIP, or Ala9-GIP for cAMP production measurement. In these series of experiments, calculated potencies (EC_{50}) were as follows: WT-GIPR-GIP, 3.7 nM; WT-GIPR-Ala3-GIP, 103 nM; R183A-GIPR-GIP, 109 nM; R183A-GIPR-Ala3-GIP, 128 nM; WT-GIPR-Ala9-GIP, 131 nM; and R183A-GIPR-Ala9-GIP, $>10^4$ nM. Values for cAMP production are expressed as a percentage of maximum cAMP production obtained with the wild-type GIPR stimulated by GIP. Results represent the means of at least three independent experiments performed in duplicate on separately transfected HEK 293 cells.

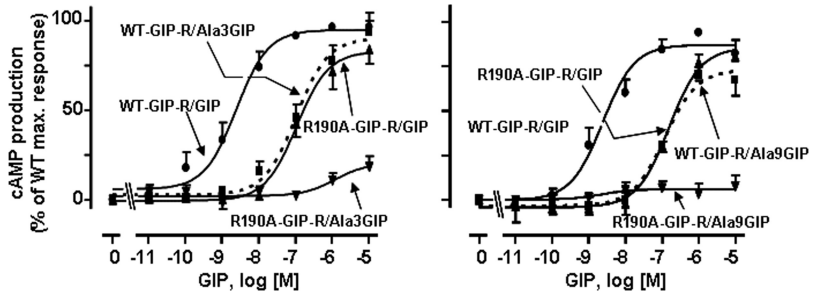

Fig. 8. Pharmacological evidence that Arg190 in GIP receptor does not interact with Glu3 or Asp9 of GIP. Wild-type GIP receptor or mutants R190A-GIPR were expressed in HEK 293 and stimulated for 15 min either by GIP, Ala3-GIP, or Ala9-GIP for cAMP production measurement. Calculated potencies (EC_{50}) were as follows: WT-GIPR-GIP, 2.4 nM; WT-GIPR-Ala3-GIP, 103 nM; WT-GIPR-Ala9-GIP, 120 nM; R190A-GIPR-GIP, 104 nM; R190A-GIPR-Ala3-GIP, $>10^4$ nM; and R190A-GIPR-Ala9-GIP, $>10^4$ nM. Values for cAMP production are expressed as percentage of maximum cAMP production obtained with the wild-type GIPR stimulated by GIP. Results represent the means of at least three independent experiments performed in duplicate on separately transfected HEK 293 cells.

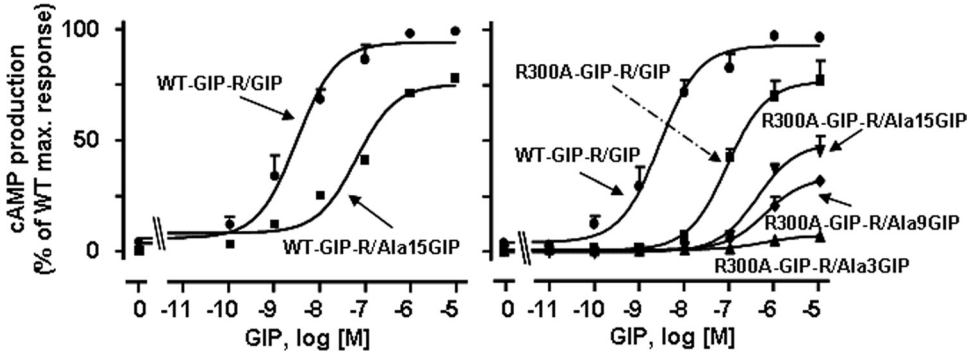

Fig. 9. Pharmacological evidence that Arg300 in GIP receptor does not interact with Glu3, Asp9, or Asp15 of GIP. HEK 293 cells expressing the wild-type GIP receptor or mutants R300A-GIPR were expressed in HEK 293 and stimulated for 15 min either by GIP, Ala3-GIP, Ala9-GIP, or Ala15-GIP for cAMP production measurement. Calculated potencies (EC_{50}) were as follows: WT-GIPR-GIP, 3.0 nM; WT-GIPR-Ala15-GIP, 63 nM; R300A-GIPR-GIP, 87 nM; R300A-GIPR-Ala3-GIP, $> 10^4$ nM; R300A-GIPR-Ala9-GIP, $>10^4$ nM; R300A-GIPR-Ala15-GIP, $>10^4$ nM. Values for cAMP production are expressed as percentage of maximum cAMP production obtained with the wild-type GIPR stimulated by GIP. Results represent the means of at least three independent experiments performed in duplicate on separately transfected HEK 293 cells.

ports the formation of a turn-like structure that fits into the narrow space between TMH 1, 2, and 7.

Concerning residues Asp9 and Asp15 of GIP, which, in the current study, have not been found to pair with amino acids of TMH in the GIPR, model B of GIPR-GIP complex shows the following interactions: Asp9 interacts with Asn283 and Arg289 in ECL2, which are two amino acids located downstream and upstream, respectively, of Cys286 in ECL2; Asp15 is involved in interactions with the N terminus of the ECD and intramolecularly with Gln19 in GIP, a result that corresponds to what has been found in the X-ray structure (Parthier et al., 2007).

Discussion

Owing to the high importance of members of group B of the GPCR family in physiology, the understanding of the mechanism by which they are activated by their natural ligands and the discovery of nonpeptide ligands for those receptors represent timely challenges. Identification of ligand binding sites represents a key step that should greatly help to take up these challenges. In the current study, our aim was to gain insight into the binding site of human GIPR, with a special focus on residues that were expected to interact with the N-terminal portion of GIP. According to structure-activity relationship data and the recent crystal structure of the complex formed between GIPR ECD and GIP, these residues are the most fundamental for receptor activation but are not involved in high-affinity and selectivity binding with GIPR ECD (Parthier et al., 2007). Based on our past successful experience with cholecystokinin and gastrin receptors, we used in synergy molecular modeling to propose candidates in both receptor and ligand and applied site-directed mutagen-

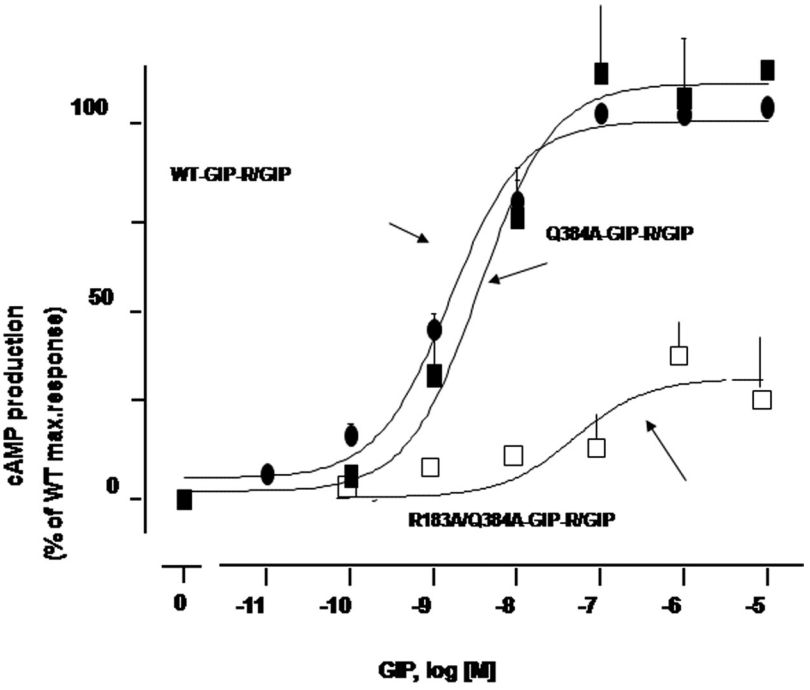

Fig. 10. Effects of single mutation Gln384Ala and double mutation R183A-Q384A on GIP-induced cAMP production. HEK 293 cells expressing the wild-type GIP receptor or mutants were expressed in HEK 293 cells and stimulated for 15 min by GIP for cAMP production measurement. Calculated potencies (EC_{50},) were as follows: WT-GIPR, 1.96 ± 0.32 nM; Q384A-GIPR, 5.2 ± 1.4 nM; and R183A-Q384A-GIPR, 32.5 ± 12.3 nM. Values for cAMP production are expressed as a percentage of maximum cAMP production obtained with the wild-type GIPR stimulated by GIP. Results represent the means of at least three independent experiments performed in duplicate on separately transfected HEK 293 cells. It is worthy to note that expression level of double mutant was only 12% of that of WT-GIPR.

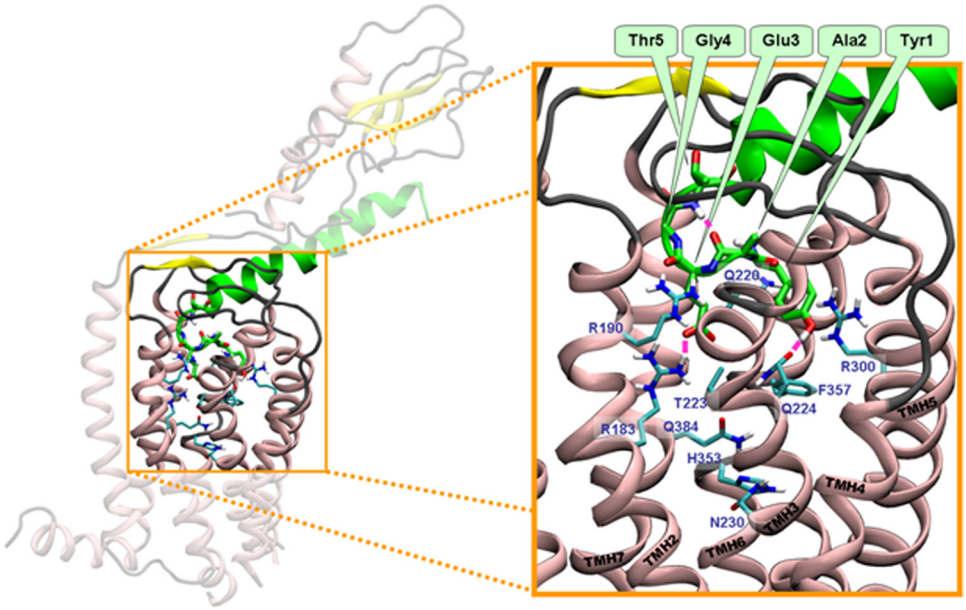

Fig. 11. Model of the interactions of GIP N terminus in the binding pocket of GIPR. The ligand receptor interaction follows binding model B, which has been identified as most suitable to explain our experimental data. Important GIPR residues in ligand binding are shown in atom colors with cyan carbons. Residues of the GIP N terminus involved in these interactions are shown in atom colors with green carbons. Hydrogen bond contacts, which remained stable during molecular dynamics simulation, are shown as magenta lines. Tyr1 of GIP establishes a hydrogen bond to Gln224 (TMH3) and π-cation interaction to the guanidino group of Arg300 (TMH5). It also rests in a hydrophobic pocket containing Phe357 (TMH6) as main contributor. The GIP Glu3 interacts with Arg183 (TMH2). Hydrogen bonding between the Glu3 backbone NH with the side-chain carbonyl of Gln220 (TMH3) is possible (not shown). The small side chain of the GIP Gly4 allows a close orientation to TMH1 in the narrow space between TMH2 and TMH7.

esis to pharmacologically evaluate theoretical predictions (Gigoux et al., 1999; Silvente-Poirot et al., 1999). For pharmacological characterization of the interactions, we analyzed the impact of receptor mutations on cAMP production rather than on binding of radioiodinated GIP, because we intended to identify amino acids involved in ligand-dependent receptor activation and because there are discrepancies between contribution to affinity and to activity of amino acids analyzed (Hinke et al., 2001; Gault et al., 2007). Moreover, radioiodination of GIP requires modification of Tyr1, a critical residue that is likely to be directly involved in GIPR activation.

GIP was initially docked in our GIPR models orienting its N terminus in different potential binding modes based on information on GPCR binding sites as well as on photolabeling investigations of secretin and glucagon in their corresponding receptors (Runge et al., 2003; Dong et al., 2008). Taking into account experimental data on other class B GPCRs, as well as the recently identified interaction of GIP in the GIPR ECD, an orientation of the N-terminal portion of GIP between TMH2 and TMH3, as well as TMH6 and TMH7 has been selected as most suitable. Pharmacological analysis of GIPR mutants, moreover, are in favor of the binding site for the GIP N terminus in which Glu3 in GIP is in functional interaction with Arg183 and biologically crucial Tyr1 interacts with Gln224 (TMH3), Arg300 (TMH5), and Phe357 (TMH6). To our knowledge, such precise structural information on this area of the GIPR binding site was not available yet. Theoretical data from a modeling study has been reported (Malde et al., 2007) but the study lacks experimental validation and is not in agreement with results from our experiments.

Interaction of Arg183 in GIPR with Glu3 in GIP seems crucial for agonist-induced receptor activation. It is noteworthy that this receptor residue is conserved within all members of subfamily B1, and there is now general agreement for its interaction with the amino acid located in position 3 in the cognate ligands. For example, in the rat secretin receptor, substitution of Arg166 equivalent to Arg183 in the GIPR also dramatically decreased the potency of secretin to stimulate cAMP production, and this residue was shown to interact with Asp3 of secretin. In the VPAC1 and VPAC2 receptors, the mutation of the corresponding basic amino acids was reported to affect potency of VIP to stimulate the receptors (Solano et al., 2001; Vertongen et al., 2001). As for rat secretin receptor, pharmacological analysis of the mutants using substituted peptide analogs provided evidence that Asp3 in VIP was likely to be interacting with a basic amino acid equivalent to Arg183 in the GIPR. In the PTH1 and PTH2 receptors, Arg233 and Arg190 equivalent to Arg183 in the GIPR were also shown to be critical for high-affinity binding of PTH and high potency activation of the receptors (Gardella et al., 1996; Turner et al., 1998).

On the contrary to Arg183, Arg190 in GIPR was not found to interact directly with an acidic residue of the ligand, although it is also critical for potency by which GIP induces cAMP. Residues equivalent to Arg190 were reported to be important in other members of group B1 GPCRs and were proposed to act as a selectivity filter in ligand recognition for GL, SCT, and VIP receptors (Di Paolo et al., 1998; Perret et al., 2002; Waelbroeck et al., 2002). Indeed, a negative charge is conserved in position 3 of ligand peptides GIP, SCT, VIP, pituitary adenylyl cyclase-activating protein, growth hormone-releasing hormone, GLP1, and GLP2, but not in GL. The corresponding receptors of these peptides, but not GL-R, share two positive charges in the corresponding positions to Arg190 and Arg183 in GIPR. In contrast, in GL-R, only Lys187 in TMH2, the positive charge corresponding to the GIPR Arg183, is conserved, whereas the amino acid corresponding to the GIPR Arg190 is the uncharged residue isoleucine. Therefore, there is a correlation between the absence of a second positive charge in TMH2 of GL-R (compared with other class B GPCRs) and the presence of the uncharged Gln3 in GL, supporting the idea that the basic residue corresponding to Arg190 in the GIPR may play a role of selective filter in group B1 GPCRs.

In the PTH2 receptor, Arg233, equivalent to Arg183 in

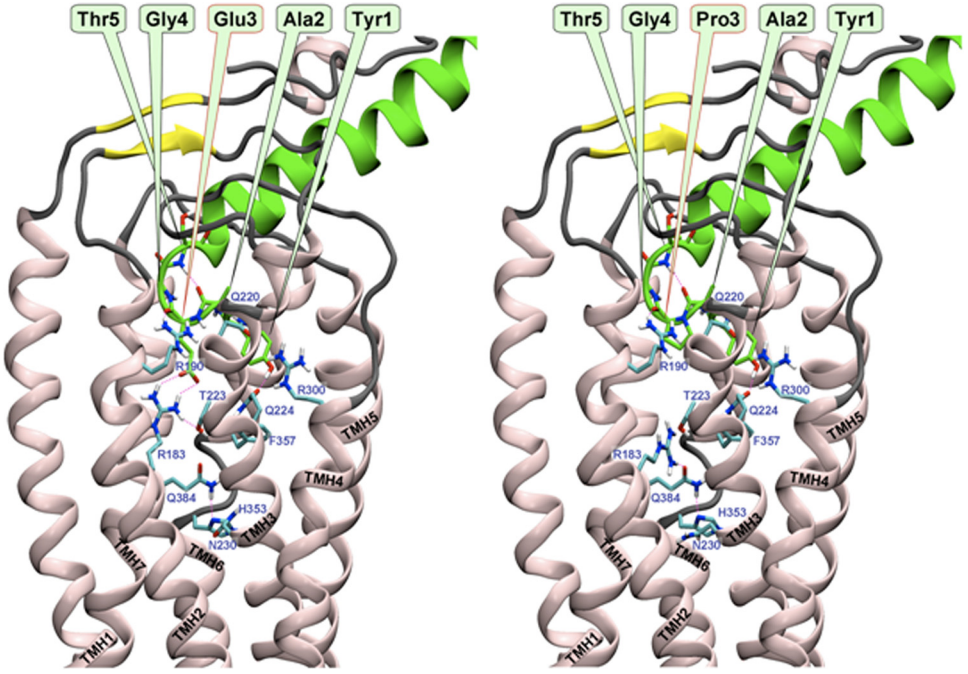

Fig. 12. Comparison between models of N terminus docking of GIP and its antagonistic derivative E3P-GIP in the GIPR binding site. Ligand and receptor orientation and representation follow the style in Fig. 11. Pro3 in E3P-GIP supports the formation of the turn-like structure we suggest to be crucial in GIP-GIPR interaction. However, the E3P-GIP lacks the positive charge in position 3, which is important in receptor activation by interaction with Arg183 in TMH2. The comparison between the native GIP (left) and its antagonistic derivative E3P-GIP (right) clearly indicates that, because of substitution of Glu3 to proline, Arg183 does not interact with the ligand. Instead, Arg183 interacts with Gln384 in TMH7, thus constraining the receptor in an inactive state.

GIPR, was shown to be functionally linked to a conserved reside of helix VII, namely Gln451 (Gardella et al., 1996). In the PTH2 receptor, exchange of Gln451 for a Lys reduced the binding affinity of PTH, and when this mutation was combined with that of Arg233 in helix II, binding affinity of the double mutant for PTH was almost restored, but no more cAMP production could be detected (Gardella et al., 1996). Although in the case of GIPR, a different situation seems to occur, our modeling and experimental results with GIPR also strongly support spatial proximity and functional link between conserved Arg of helix II and Gln of helix VII. In the current study, we show that the alanine exchange of the conserved Gln of helix VII, namely Gln384, decreased the potency with which GIP stimulates its receptor by 2.6-fold (Table 1). Introducing a double mutation of Arg183 and Gln384 in GIPR caused a smaller shift in potency than single mutation of Arg183 but dramatically decreased the apparent efficacy with which the GIPR responded to GIP, a result that may be due to the drop of expression of double-mutant as a functional receptor at the cell surface.

Another important new finding provided by the current study concerns residues in functional interaction with Tyr1 of GIP, which were found located in three different TMH of the GIPR. These are Arg300 (TMH5), Phe357 (TMH6), and Gln224 (TMH3), which seem, in the model, to bind GIP Tyr1 through π-cation interaction, hydrophobic contacts, and a hydrogen bond, respectively. Although sequence alignment investigations of subfamily B1 GPCRs indicate a high degree of conservation of these three amino acids in class B of GPCRs, analysis of the cognate ligands shows the presence of a tyrosine at position 1 only in GIP and GRF, whereas other ligands have an histidine at this position. It is likely that, because of differences in physicochemical properties, Tyr1 of GIP involves a unique network of interactions in GIPR. This may explain why mutation of Arg277 in rat SCT receptor corresponding to Arg300 in GIPR does not affect SCT-induced cAMP production (Di Paolo et al., 1999).

Our data on GIP-GIPR interaction shows another particularity: the formation of a turn-like structure made-up by residues Ala2-Glu3-Gly4-Thr5. We think that the small but significant effects on ligand-induced receptor activation in Gln220 and Thr223 mutants support a turn-like conformation of the GIP N terminus. Gln220- and Thr223- in TMH3 provide a favorable environment for a turn-like structure of GIP. This observation is in agreement with the idea that the N termini of class B1 receptor peptide ligands have to adopt a specific conformation to finally activate their receptor (Neumann et al., 2008). This hypothesis, together with the finding that Arg183 in GIPR interacts with Glu3 in GIP, allows us to propose a possible explanation for the substitution of Glu3 to proline in GIP resulting in an antagonistic ligand for GIPR (Gault et al., 2002). Indeed, we suggest that this substitution favors the formation of a turn-like structure established by residues Ala2-Pro3-Gly4-Thr5, which subsequently finds good interactions within the GIPR binding pocket while maintaining the receptor in an inactive state (Fig. 12).

So far, and unlike members of group A GPCRs, the mechanism by which members of group B are activated by their cognate ligands remains poorly documented. Viewed from a structural perspective, these receptors lack conserved motifs and residues such as E/DRY, NPXXY motifs, which have been involved in the activation process of group A GPCRs. However, a general mechanism of peptide ligand interaction with class B GPCRs has emerged, termed the "two-domain" model, in which the C-terminal moiety of the ligand binds with a high affinity and selectivity to receptor ECD within a period of time less than 140 ms followed by slower binding of ligand N-terminal to TMH of the receptor to activate it and triggers G protein coupling (Castro et al., 2005). The precise underlying mechanisms corresponding to this second step remain to be elucidated. However, it is plausible to consider that part of the binding site formed by the TMH core could be targeted by appropriate nonpeptide ligands, as has been possible for most class A GPCRs, and therefore will be amenable to medicinal chemistry. Future work will be dedicated to the refinement of the modeled structure of this region of the GIP binding site in GIPR and to the understanding of the activation mechanism in GIPR.

Acknowledgments

We thank Bernard Thorens (Lausanne, Switzerland) who provided the cDNA encoding the human GIPR, and Bernard Monsarrat and Carole Pichereaux (Genotoul proteomic, Toulouse), who performed GIP-Alexa Fluor 647 analysis.

References

Baggio LL and Drucker DJ (2007) Biology of incretins: GLP-1 and GIP. *Gastroenterology* **132:**2131–2157.
Ballesteros JA and Weinstein H (1995) Integrated methods for the construction of three dimensional models and computational probing of structure-function relations in G-protein coupled receptors. *Methods Neurosci* **25:**366–428.
Betancourt MR and Thirumalai D (1999) Pair potentials for protein folding: choice of reference states and sensitivity of predicted native states to variations in the interaction schemes. *Protein Sci* **8:**361–369.
Brown JC (1974) Candidate hormones of the gut. 3. Gastric inhibitory polypeptide (GIP). *Gastroenterology* **67:**733–734.
Castro M, Nikolaev VO, Palm D, Lohse MJ, and Vilardaga JP (2005) Turn-on switch in parathyroid hormone receptor by a two-step parathyroid hormone binding mechanism. *Proc Natl Acad Sci USA* **102:**16084–16089.
Chenna R, Sugawara H, Koike T, Lopez R, Gibson TJ, Higgins DG, and Thompson JD (2003) Multiple sequence alignment with the Clustal series of programs. *Nucleic Acids Res* **31:**3497–3500.
Di Paolo E, De Neef P, Moguilevsky N, Petry H, Bollen A, Waelbroeck M, and Robberecht P (1998) Contribution of the second transmembrane helix of the secretin receptor to the positioning of secretin. *FEBS Lett* **424:**207–210.
Di Paolo E, Vilardaga JP, Petry H, Moguilevsky N, Bollen A, Robberecht P, and Waelbroeck M (1999) Role of charged amino acids conserved in the vasoactive intestinal polypeptide/secretin family of receptors on the secretin receptor functionality. *Peptides* **20:**1187–1193.
Dong M, Gao F, Pinon DI, and Miller LJ (2008) Insights into the structural basis of endogenous agonist activation of family B G protein-coupled receptors. *Mol Endocrinol* **22:**1489–1499.
Dufresne M, Seva C, and Fourmy D (2006) Cholecystokinin and gastrin receptors. *Physiol Rev* **86:**805–847.
Gardella TJ, Luck MD, Fan MH, and Lee C (1996) Transmembrane residues of the parathyroid hormone (PTH)/PTH-related peptide receptor that specifically affect binding and signaling by agonist ligands. *J Biol Chem* **271:**12820–12825.
Gault VA, Hunter K, Irwin N, Green BD, Greer B, Harriott P, O'Harte FP, and Flatt PR (2007) Characterisation and biological activity of Glu3 amino acid substituted GIP receptor antagonists. *Arch Biochem Biophys* **461:**263–274.
Gault VA, O'Harte FP, Harriott P, and Flatt PR (2002) Characterization of the cellular and metabolic effects of a novel enzyme-resistant antagonist of glucose-dependent insulinotropic polypeptide. *Biochem Biophys Res Commun* **290:**1420–1426.
Gether U (2000) Uncovering molecular mechanisms involved in activation of G protein-coupled receptors. *Endocr Rev* **21:**90–113.
Gigoux V, Escrieut C, Fehrentz JA, Poirot S, Maigret B, Moroder L, Gully D, Martinez J, Vaysse N, and Fourmy D (1999) Arginine 336 and asparagine 333 of the human cholecystokinin-A receptor binding site interact with the penultimate aspartic acid and the C-terminal amide of cholecystokinin. *J Biol Chem* **274:**20457–20464.
Gremlich S, Porret A, Hani EH, Cherif D, Vionnet N, Froguel P, and Thorens B (1995) Cloning, functional expression, and chromosomal localization of the human pancreatic islet glucose-dependent insulinotropic polypeptide receptor. *Diabetes* **44:**1202–1208.
Hinke SA, Gelling R, Manhart S, Lynn F, Pederson RA, Kühn-Wache K, Rosche F, Demuth HU, Coy D, and McIntosh CH (2003) Structure-activity relationships of glucose-dependent insulinotropic polypeptide (GIP). *Biol Chem* **384:**403–407.
Hinke SA, Manhart S, Pamir N, Demuth H, W Gelling R, Pederson RA, and McIntosh CH (2001) Identification of a bioactive domain in the amino-terminus of glucose-dependent insulinotropic polypeptide (GIP). *Biochim Biophys Acta* **1547:**143–155.

Hinke SA, Manhart S, Speck M, Pederson RA, Demuth HU, and McIntosh CH (2004) In depth analysis of the N-terminal bioactive domain of gastric inhibitory polypeptide. *Life Sci* **75:**1857–1870.
Horn F, Bettler E, Oliveira L, Campagne F, Cohen FE, and Vriend G (2003) GPCRDB information system for G protein-coupled receptors. *Nucleic Acids Res* **31:**294–297.
Jaakola VP, Griffith MT, Hanson MA, Cherezov V, Chien EY, Lane JR, Ijzerman AP, and Stevens RC (2008) The 2.6 angstrom crystal structure of a human A2A adenosine receptor bound to an antagonist. *Science* **322:**1211–1217.
Jörnvall H, Carlquist M, Kwauk S, Otte SC, McIntosh CH, Brown JC, and Mutt V (1981) Amino acid sequence and heterogeneity of gastric inhibitory polypeptide (GIP). *FEBS Lett* **123:**205–210.
Kieffer TJ (2003) GIP or not GIP? That is the question. *Trends Pharmacol Sci* **24:**110–112.
Malde AK, Srivastava SS, and Coutinho EC (2007) Understanding interactions of gastric inhibitory polypeptide (GIP) with its G-protein coupled receptor through NMR and molecular modeling. *J Pept Sci* **13:**287–300.
Mentlein R, Gallwitz B, and Schmidt WE (1993) Dipeptidyl-peptidase IV hydrolyses gastric inhibitory polypeptide, glucagon-like peptide-1(7–36)amide, peptide histidine methionine and is responsible for their degradation in human serum. *Eur J Biochem* **214:**829–835.
Moody AJ, Thim L, and Valverde I (1984) The isolation and sequencing of human gastric inhibitory peptide (GIP). *FEBS Lett* **172:**142–148.
Murphy LR, Wallqvist A, and Levy RM (2000) Simplified amino acid alphabets for protein fold recognition and implications for folding. *Protein Eng* **13:**149–152.
Neumann JM, Couvineau A, Murail S, Lacapère JJ, Jamin N, and Laburthe M (2008) Class-B GPCR activation: is ligand helix-capping the key? *Trends Biochem Sci* **33:**314–319.
Parthier C, Kleinschmidt M, Neumann P, Rudolph R, Manhart S, Schlenzig D, Fanghänel J, Rahfeld JU, Demuth HU, and Stubbs MT (2007) Crystal structure of the incretin-bound extracellular domain of a G protein-coupled receptor. *Proc Natl Acad Sci USA* **104:**13942–13947.
Perret J, Van Craenenbroeck M, Langer I, Vertongen P, Gregoire F, Robberecht P, and Waelbroeck M (2002) Mutational analysis of the glucagon receptor: similarities with the vasoactive intestinal peptide (VIP)/pituitary adenylate cyclase-activating peptide (PACAP)/secretin receptors for recognition of the ligand's third residue. *Biochem J* **362:**389–394.
Runge S, Wulff BS, Madsen K, Bräuner-Osborne H, and Knudsen LB (2003) Different domains of the glucagon and glucagon-like peptide-1 receptors provide the critical determinants of ligand selectivity. *Br J Pharmacol* **138:**787–794.
Silvente-Poirot S, Escrieut C, Galès C, Fehrentz JA, Escherich A, Wank SA, Martinez J, Moroder L, Maigret B, Bouisson M, et al. (1999) Evidence for a direct interaction between the penultimate aspartic acid of cholecystokinin and histidine 207, located in the second extracellular loop of the cholecystokinin B receptor. *J Biol Chem* **274:**23191–23197.
Solano RM, Langer I, Perret J, Vertongen P, Juarranz MG, Robberecht P, and Waelbroeck M (2001) Two basic residues of the h-VPAC1 receptor second transmembrane helix are essential for ligand binding and signal transduction. *J Biol Chem* **276:**1084–1088.
Turner PR, Mefford S, Bambino T, and Nissenson RA (1998) Transmembrane residues together with the amino terminus limit the response of the parathyroid hormone (PTH) 2 receptor to PTH-related peptide. *J Biol Chem* **273:**3830–3837.
Vertongen P, Solano RM, Perret J, Langer I, Robberecht P, and Waelbroeck M (2001) Mutational analysis of the human vasoactive intestinal peptide receptor subtype VPAC(2): role of basic residues in the second transmembrane helix. *Br J Pharmacol* **133:**1249–1254.
Volz A, Göke R, Lankat-Buttgereit B, Fehmann HC, Bode HP, and Göke B (1995) Molecular cloning, functional expression, and signal transduction of the GIP-receptor cloned from a human insulinoma. *FEBS Lett* **373:**23–29.
Waelbroeck M, Perret J, Vertongen P, Van Craenenbroeck M, and Robberecht P (2002) Identification of secretin, vasoactive intestinal peptide and glucagon binding sites: from chimaeric receptors to point mutations. *Biochem Soc Trans* **30:**437–441.

Address correspondence to: Daniel Fourmy, U858 INSERM I2MR, equipe 13, 1 avenue Jean Poulhès, BP 84225, 31432 Toulouse Cedex 4, France. E-mail: daniel.fourmy@inserm.fr